Optimal Power Flow Control in Parallel Operating AC and DC Distribution Links

Shekhar, Aditya; Soeiro, Thiago Batista; Wu, Yang; Bauer, Pavol

DOI
10.1109/TIE.2020.2970675

Publication date
2021

Document Version
Accepted author manuscript

Published in
IEEE Transactions on Industrial Electronics

Optimal Power Flow Control in Parallel Operating AC and DC Distribution Links

Aditya Shekhar, *Student Member*, Thiago Batista Soeiro, *Member*,
Yang Wu, *Student Member*, and Pavol Bauer, *Senior Member*

***Abstract*—DC links with back to back voltage source converters are usually built alongside the existing medium voltage ac distribution grids for infrastructure reinforcement. The distribution network operators need to run multiple of such parallel ac and dc links between two substations at optimal efficiency. This paper shows that the active power steering capability of the dc link can be used to dynamically vary the share of power flow in the ac link such that the system operating efficiency is maximized for varying power demand, grid voltage, dc link voltage, converter efficiency, link length and conductor area. The algorithm developed based on the derived exact and estimated solution for this parallel ac-dc link power sharing ratio is proved through simulations on a 10 kV, 30 MVA system. The concept is validated using experiments on a scale-down lab model. Using case-study with adapted measured substation data of hourly average power demand profile for one year, it is shown that annual energy saving potential in the range of 8-92 MWh can be achieved with varying link length between 10-20 km for 5-20 kV grid voltage and 185-630 mm^2 conductor area if the proposed optimal power flow control is used.**

NOMENCLATURE

A_{con}	Cross-sectional area of a single link conductor.
E_{loss}	Total system energy loss over one year of operation.
i_{ac}, i_{dc}	Single ac and dc conductor current respectively.
k_{e}	Operating voltage ratio between dc & ac conductor.
l	Distance between sending and receiving substation.
N_{ac}	Number of conductors under ac operation.
N_{dc}	Number of conductors under dc operation.
$P_{\text{L,cond}}$	Total ohmic power loss in link conductors.
$P_{\text{L,conv}}$	Total converter power loss.
$P_{\text{L,sys}}$	Total operating power loss of the system.
r_{ac}, r_{dc}	Single ac and dc conductor resistance in Ω/km.
$R_{\text{cond,i}}$	Conductor operating resistance at i$^{\text{th}}$ iteration.
$R_{90^\circ\text{C}}$	Conductor resistance at 90°C.
$S_{\text{conv,SSS}}$	Demand at the sending end converter station.
$S_{\text{conv,RSS}}$	Demand met by the receiving end converter station.
S_{RSS}	Apparent power demand at receiving substation.
T_{amb}	Ambient temperature.
T_{ac}, T_{dc}	Single ac and dc conductor operating temperature.
$T_{\text{cond,i}}$	Conductor operating temperature at i$^{\text{th}}$ iteration.
$V_{\text{LL,rms}}$	Line to line r.m.s. substation ac bus voltage.
V_{d}	Voltage of the dc link.
y	Ratio of active dc power flow to that of the total active power demand at system receiving end.
y_{con}	y computed based on the ratio of active power capacity of the dc and ac link conductors.
y_{opt}	y for optimal system operating efficiency.
η_{SSS}, η_{RSS}	Efficiency of sending and receiving end converters.
α	Temperature coefficient of the link conductor.
$\cos\theta$	Receiving end operating power factor.

Manuscript received Month xx, 2xxx; revised Month xx, xxxx; accepted Month x, xxxx. This work is funded by tki switch2smartgrids under the project Flexible and Future Power Links (FLINK) for Smart Grids for Rijksdienst voor Ondernemend, Nederland.

The authors are with the Department of Electrical and Computer Engineering, Delft University of Technology, The Netherlands, e-mail: a.shekhar@tudelft.nl, ashekhr@gmail.com.

I. INTRODUCTION

Energy transition goals have increased the reliance on the electrical grid and thus, imposed new requirements on the existing alternating-current (ac) transmission and distribution network infrastructure. A recent white-paper emphasizes the role of utility interfaced power electronics assisted direct-current (dc) technologies in addressing many of these challenges, particularly in medium voltage distribution networks [1]. For example, the use of dc interlinks in supporting the ac power systems with bidirectional active power redirection, ancillary services and power outage management is explored in [2]–[5]. Further, it has been investigated that converting existing ac distribution links to operate under dc conditions can increase the capacity of the system [6], [7].

A. Motivation

Fig. 1 shows a simplified illustration of a parallel operating ac and dc link structure that will emerge as such applications are employed to restructure the grids.

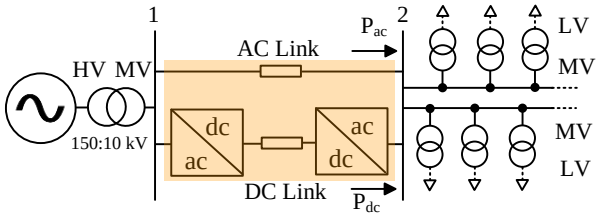

Fig. 1: Illustration of parallel operating dc and ac links.

The highlighted parallel ac-dc link is shown between bus '1' and '2' of a Medium voltage (MV) network section which interconnects the High Voltage (HV) transmission network to a downstream radial MV distribution grid subsequently to Low

Voltage (LV) grids. The operating efficiency at this point-to-point link is important because it supports the high power demand of the entire downstream network and can be few tens of kilometers long [8]. Further, the ac and dc link losses disproportionately and dynamically vary with receiving end active and reactive power demand, ac grid voltage, dc link voltage, converter efficiency, link length and conductor area.

B. Literature Review

The bulk active power routing and reactive power support functionality of ac grid connected Back-To-Back Voltage Source Converter (B2B-VSC) based dc link has been explored in detail in [9]–[12]. However, with an ac link operating in parallel, the ability of the VSC to steer power in both the ac and dc paths can be utilized to maximize the operating efficiency of the system while supporting the full reactive power needs at node '2'. Fundamentally, the principle of optimal power sharing is similar to the concept applied for parallel converters [13], but with some key differences; such as (i) The losses in the ac and dc power flow paths depend on dissimilar factors. For example, while there are no converter losses in the ac path, dc link conductor losses are relatively lower for a given power [6] (ii) The functionality, and therefore the converter losses on each side of the B2B-VSC are different. For example, the reactive power demand at the receiving end node is fully supported by the respective VSC operating as an inverter while the sending end rectifier is operating in voltage control mode (iii) Since the distance between Node 1 and Node 2 (ref. Fig. 1) can be in few kilometers, relatively less locally measured information is available with receiving-end converter controller. The demonstration of power-electronic based realization of the optimal power flow algorithm with dynamically varying network operating conditions is therefore, an important focus of this work.

In [14], an integrated optimal power flow model is derived for a hybrid ac/dc grid with focus on implementation. The paper explores the trade-offs between accuracy and speed of the derived model for different problem sizes. For an urban distribution network with few existing lines refurbished from ac to dc operation, [15] optimizes the system topology of the resultant hybrid ac/dc grid considering investments and power losses while accommodating renewable energy resources and fully utilizing the transfer capacity. Network reconfigurability of a hybrid ac-dc distribution grid is explored for optimal operation by using a communication based two-stage energy management system in [16]. The paper reported cost savings of 2.35 % and loss reduction of 9.75 % with the proposed optimization for a given test case of 24 hour operation in a 33-bus system. A decentralized optimization method is mathematically developed in [17] and its convergence properties are explored both theoretically and experimentally in practical hybrid ac/dc grids. Convergence properties of optimal power flow are further explored in [18], wherein a N-node ac/dc grid is partitioned and decoupled by distinguishing between ac and dc nodes and their interfacing infrastructure. While significant research has been established for optimization and implementation of power flow models in hybrid ac/dc grids, more insight on the potential of optimal power flow with varying grid parameters can be of value, particularly for applications in restructuring, refurbishing and reconfiguration of such networks for varied operating conditions.

C. Key Contributions

The main objective of this paper is to highlight the potential of power sharing between point to point parallel ac and dc distribution links that can be either reconfigurable or fixed, to maximize system efficiency for varying operating conditions and demonstrate the concept with simulations, experiments and case-study with adapted substation data. The specific contributions of the work are as follows:

- Derive the analytical expression for optimal ac-dc active power sharing ratio to gain insight on the dependence with number of ac and dc conductors in the re-configurable link, dc link voltage enhancement, grid voltage, apparent power demand, power factor, converter efficiency, link length and conductor cross-sectional area.
- Describe the potential energy savings with the proposed method by performing sensitivity analysis using a case-study with adapted annual operational data from an existing distribution network link.
- Show simulated system operation with deployment of optimal active power sharing algorithm and reactive power support using converter control.
- Develop experimental proof-of concept including supporting evidence for the predicted tendencies and critical comparison with theoretically estimated values.

D. Structure of the Paper

Section II describes the system studied and derives the system losses as a function of various operating parameters to establish the concept of optimal power flow for maximizing efficiency. In Section III, the analytic expression of optimal dc power ratio is derived and the estimated value is compared with the exact value for different operating powers and link lengths. In Section IV, the optimal power flow control algorithm is developed and simulations are performed to prove the working of the concept. Using case-study with adapted measured substation data of hourly average power demand profile for one year, Section V determines the annual energy saving potential for varying grid voltages, link length and conductor area. Section VI presents the experimental insight on the concept using a lab-scale model. Section VII offers concluding remarks on the key contributions and future research directions.

II. Background on Active Power Sharing and Optimal System Efficiency

A. System Description

In Fig. 2, the system diagram is shown for a parallel ac-dc link of a given length 'l' between Sending-end Substation (SSS) and Receiving-end Substation (RSS). Such an arrangement can be present in transmission and distribution networks as suggested in [6].

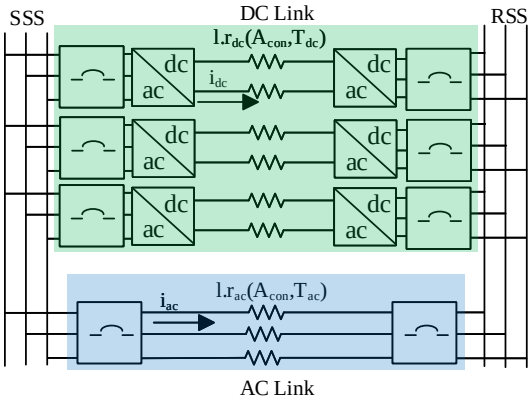

Fig. 2: Schematic Diagram of parallel operating dc and ac links.

Table II lists the system parameters that are used for the presented results and correspond to the refurbishment strategy of a benchmark ac distribution link system described in [19]. The base power physically describes the rated capacity of a single 3-phase ac link in the system. The subsequent subsections describe the losses in the system that are derived in detail in [6] and develop insight on optimal power sharing for maximizing operating efficiency.

B. Link Conductor Losses

For the given RSS power demand (S_{RSS}) at power factor (pf=$\cos\theta$), let the share of active power delivered by the dc link be y within the capacity constraints explained in [6]. Considering that the RSS-side VSCs support the full load reactive power demand, the power transferred by the ac and dc links are $[(1-y)S_{\text{RSS}}\cos\theta]$ and $[yS_{\text{RSS}}\cos\theta]$, respectively. With number of ac and dc link conductors N_{ac} and N_{dc}, the conductor currents i_{ac} and i_{dc} are described by (1) and (2), respectively.

$$i_{\text{ac}} = \frac{(1-y)S_{\text{RSS}}\cos\theta}{\left(\frac{N_{\text{ac}}}{3}\right)\sqrt{3}V_{\text{LL,rms}}} = \frac{\sqrt{3}(1-y)S_{\text{RSS}}\cos\theta}{N_{\text{ac}}V_{\text{LL,rms}}} \quad (1)$$

$$i_{\text{dc}} = \frac{yS_{\text{RSS}}\cos\theta}{\left(\frac{N_{\text{dc}}}{2}\right)V_{\text{d}}} = \frac{\sqrt{3}yS_{\text{RSS}}\cos\theta}{N_{\text{dc}}k_{\text{e}}V_{\text{LL,rms}}} \quad (2)$$

Herein, k_{e} corresponds to the ratio of line to line ac grid voltage $V_{\text{LL,rms}}$ and dc link voltage V_{d} as described by (3),

$$V_{\text{d}} = \frac{2k_{\text{e}}V_{\text{LL,rms}}}{\sqrt{3}} \quad (3)$$

V_{d} is controlled by the SSS converter for a constant k_{e} chosen in accordance with the operational requirements of the system. The total ohmic conductor losses ($P_{\text{L,cond}}$) are therefore given by (4),

$$P_{\text{L,cond}} = N_{\text{ac}}i_{\text{ac}}^2 lr_{\text{ac}}(A_{\text{con}},T_{\text{ac}}) + N_{\text{dc}}i_{\text{dc}}^2 lr_{\text{dc}}(A_{\text{con}},T_{\text{dc}}) \quad (4)$$

For a particular conductor current I_{cond}, the operating temperature $T_{\text{cond,k}}$ and conductor resistance $R_{\text{cond,k}}$ are iteratively computed based on (5) and (6) respectively.

$$T_{\text{cond,i}} = T_{\text{amb}} + \left(\frac{I_{\text{cond}}^2 R_{\text{cond,i-1}}}{I_{\text{rated}}^2 R_{90^\circ\text{C}}}\right)(90 - T_{\text{amb}}) \quad (5)$$

$$R_{\text{cond,i}} = R_{90^\circ\text{C}}\left(\frac{1+\alpha(T_{\text{cond,i}} - T_{\text{amb}})}{1+\alpha(90 - T_{\text{amb}})}\right) \quad (6)$$

'i' is the iteration step, T_{amb} is the ambient temperature, $R_{90^\circ\text{C}}$ is the resistance of the conductor in Ω/km at 90°C and α is the temperature coefficient. $R_{\text{Tcond,0}}$ is the initial conductor resistance assumed equal to $R_{90\text{C}}$. Fig. 3 shows the operating parameters of the ac and dc link conductors for different S_{RSS} at pf=0.9 with varying y.

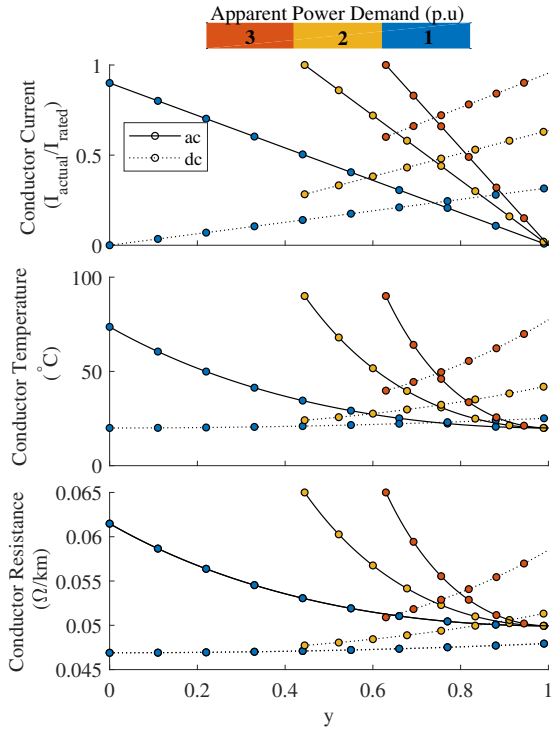

Fig. 3: Estimated operating current, temperature and resistance for ac and dc link conductors for different RSS apparent power demand at pf=0.9 with varying y.

The observed variations in currents and temperature, and therefore the resistances are in part due to the conductor utilization corresponding to y, N_{ac} and N_{dc}; and in part due to dc voltage enhancement factor k_{e}. The conductor utilization is maximum for the operating point $y = y_{\text{con}}$, at which the ac and dc link conductor currents are equal. This can be derived be equating (1) and (2), given by (7).

$$y_{\text{con}} = \frac{k_{\text{e}}N_{\text{dc}}}{N_{\text{ac}} + k_{\text{e}}N_{\text{dc}}} \quad (7)$$

Due to differences in operating conditions for ac and dc links, the respective conductor resistances can be different even though A_{con} is equal for both, leading to a small shift in the optimal efficiency point. The total system efficiency is also influenced by the losses in the dc link converters resulting

in a dynamic shift in the optimum dc to ac active power ratio (y_{opt}), as shall be discussed in Section II-C. y_{con} is a reasonable first approximation for minimizing system losses, in particular serving as a starting value for iterative loops required for estimating the y_{opt}, as described in Section III.

C. Converter Losses

The theory presented in [20], [21] indicates that with increasing operating power and voltage, higher number of cascaded cells are favourable for optimal efficiency and performance at a given dc link voltage. The efficiency computations were performed based on the steady state analytical loss model described in [22] including switching, conduction and inductor losses and will not be repeated here in the interest of brevity. Based on the model accounting for trade-offs between performance and efficiency, it is determined that a half bridge medium voltage grid connected Modular Multilevel Converter (MMC) with 3.3 kV Insulated Gate Bipolar Transistor (IGBT) switch based 9x submodule cells is a reasonable design choice with high efficiency for this application [23], [24]. The obtained percentage load dependent efficiency curve for a 10 MVA MMC operating at 313 Hz submodule switching frequency is shown in Fig. 4.

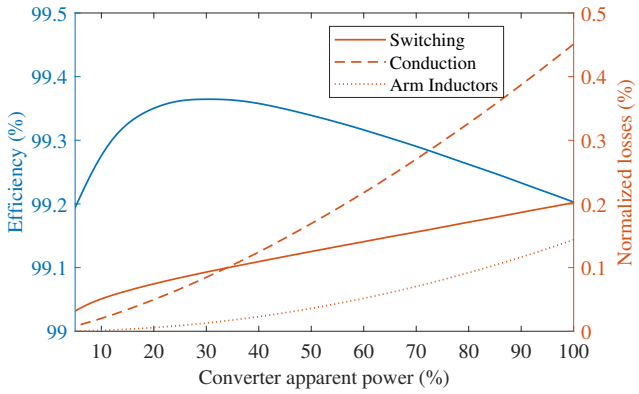

Fig. 4: Losses and Efficiency curve for DC Link modular multilevel converter with respect to loading. [6], [23], [24]

This efficiency curve is adapted based on the substation apparent demand as a percentage of the total full load capacity of the converters per substation. Some deviation in the curve can be expected with different design considerations (for example, but not limited to, the type of switches and the number of converters per substation) and operational conditions (such as switching frequency, modulation, ancillary services and RSS pf). Assuming that the reactive power demand at RSS is fully met by the substation converter, the RSS side converter demand $S_{\text{conv,RSS}}$ is given by (8).

$$S_{\text{conv,RSS}} = S_{\text{RSS}}\sqrt{y^2\cos^2\theta + \sin^2\theta} \tag{8}$$

Based on the loading, the corresponding efficiency, η_{RSS} can be selected. At the SSS side, the converter supplies the rated dc link power and the demand $S_{\text{conv,SSS}}$ is ideally approximated as (9).

$$S_{\text{conv,SSS}} = yS_{\text{RSS}}\cos\theta \tag{9}$$

In practical scenario, $S_{\text{conv,SSS}}$ is slightly higher corresponding to the losses in the dc link. The efficiency of the SSS converter at this power demand is η_{SSS}. The exact $S_{\text{conv,SSS}}$ is slightly higher corresponding to the RSS converter and dc link conductor losses. The total converter losses ($P_{\text{L,conv}}$) in the system is given by (10).

$$P_{\text{L,conv}} = (1-\eta_{\text{SSS}})S_{\text{conv,SSS}} + (1-\eta_{\text{RSS}})S_{\text{conv,RSS}} \tag{10}$$

The total system losses $P_{\text{L,sys}}$ is the summation of (4) and (10), given by (11).

$$P_{\text{L,sys}} = P_{\text{L,cond}} + P_{\text{L,conv}} \tag{11}$$

$P_{\text{L,sys}}$ as a percentage of S_{RSS} for different operating scemarios is shown in Fig. 5.

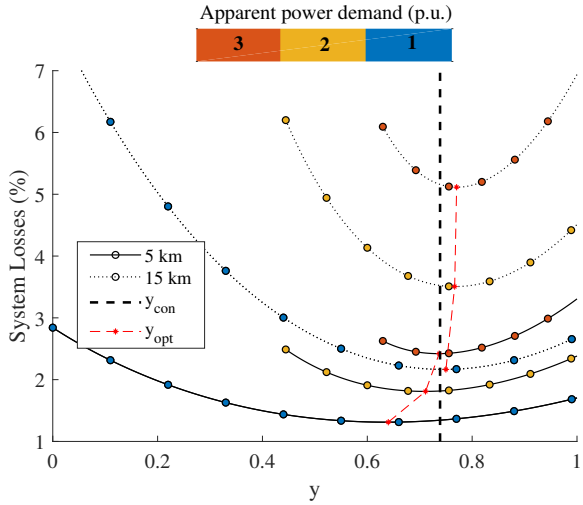

Fig. 5: System losses as function of dc power share (y) for different apparent power demand and link length at pf=0.9. The y_{opt} (dashed red) and y_{con} (dashed black) are highlighted.

It can be observed that y_{opt} increases with S_{RSS}. Furthermore, an increase in link length l increases the conductor losses but not the converter losses, thus shifting the y_{opt} in the favour of dc operation. It can be inferred that the set point for y_{opt} depends on several operating factors such as $V_{\text{ll,rms}}$, k_{e}, η, l, A_{con}, N_{ac}, N_{dc}, S_{RSS} and pf. The explored dependencies will be quantitatively derived in Section III.

III. Analytic Expression for Optimal Power Sharing Point (y_{OPT})

The analytic expression for the optimal value of y which will be derived is necessary to obtain insight on the various dependencies with variables $V_{\text{ll,rms}}$, k_{e}, η, l, A_{con}, N_{ac}, N_{dc}, S_{RSS} and pf as suggested in Section II-C. By substituting (1) and (2) in (4) and differentiating $P_{l,\text{cond}}$ with respect to y, the expression (12) is obtained.

$$\frac{\partial P_{\text{L,cond}}}{\partial y} = \left(\frac{6lS_{\text{RSS}}^2\cos^2\theta}{V_{\text{ll,rms}}^2}\right)\times \left[y\left(\frac{r_{\text{ac}}(i)}{N_{\text{ac}}} + \frac{r_{\text{dc}}(i)}{k_{\text{e}}^2\cdot N_{\text{dc}}}\right) - \left(\frac{r_{\text{ac}}(i)}{N_{\text{ac}}}\right)\right] \tag{12}$$

Since the resistance of the ac and dc link conductors ($r_{\text{ac}}(i)$,$r_{\text{dc}}(i)$) are function of y, they must be iteratively estimated based on (5) and (6). Similarly, substituting (8) and (9) in (10) and differentiating $P_{\text{L,conv}}$ with respect to y, the expression (13) is obtained.

$$\frac{\partial P_{\text{L,conv}}}{\partial y} = S_{\text{RSS}} \cos\theta[(1-\eta_{\text{SSS}}(i)) + (1-\eta_{\text{SSS}}(i))k_{\text{cf}}(i)] \tag{13}$$

$$k_{\text{cf}}(i) = \frac{y\cos\theta}{\sqrt{y^2\cos^2\theta + \sin^2\theta}} \tag{14}$$

The correction factor $k_{\text{cf}}(i)$ is a function of y, and thus, should be iteratively determined during the analytic estimation of y_{opt}. A good initial estimation for (14) is with $y = y_{\text{con}}$, where y_{con} can be found from (7). Similarly, $\eta_{\text{SSS}}(i)$ and $\eta_{\text{RSS}}(i)$ are iteratively determined functions of y. According to (11), the first derivative of total system losses $P_{\text{L,sys}}$ with respect to y can be found from (15).

$$\frac{\partial P_{\text{L,sys}}}{\partial y} = \frac{\partial P_{\text{L,cond}}}{\partial y} + \frac{\partial P_{\text{L,conv}}}{\partial y} \tag{15}$$

It can be inferred that the second derivative of $P_{\text{L,sys}}$ with respect to y, given by (16), is positive.

$$\frac{\partial^2 P_{\text{L,sys}}}{\partial y^2} = \left(\frac{6lS_{\text{RSS}}^2\cos^2\theta}{V_{\text{ll,rms}}^2}\right) \times \left(\frac{r_{\text{ac}}(i)}{N_{\text{ac}}} + \frac{r_{\text{dc}}(i)}{k_{\text{e}}^2 \cdot N_{\text{dc}}}\right) \tag{16}$$

This implies that the value of y for which (15) is equal to zero represents the minimum $P_{\text{L,sys}}$ for the specified operating conditions. The optimal efficiency point, y_{opt}, is therefore given by (17).

$$y_{\text{opt}} = \frac{1}{\left(\frac{r_{\text{ac}}(i)}{N_{\text{ac}}} + \frac{r_{\text{dc}}(i)}{k_{\text{e}}^2 \cdot N_{\text{dc}}}\right)} \left[\left(\frac{r_{\text{ac}}(i)}{N_{\text{ac}}}\right) - \left(\frac{V_{\text{LL,rms}}^2}{3lS_{\text{RSS}}\cos\theta}\right) \times \left(\frac{(1-\eta_{\text{SSS}}(i)) + (1-\eta_{\text{RSS}}(i))k_{\text{cf}}(i)}{2}\right)\right] \tag{17}$$

The analytically estimated y_{opt} using (17) with respect to S_{RSS} at pf=0.9 for link lengths of 5 km, 15 km and 30 km are shown in Fig. 6 as compared to its exact solution. The value of y_{con} is also highlighted.

As S_{RSS} increases, y_{opt} is higher, indicating a greater preference for the dc link operation. Similarly, with increasing link lengths, the dc link must operate with higher share of power for the system to operate with minimal losses. The associated dependencies of y_{opt} shift with various system parameters, as described by (17).

Suppose the actual dc link active power share is $y_{\text{act}} = y_{\text{opt}} + \Delta y$, the deviation Δy from y_{opt} can occur due to a number of reasons, one of them associated with the constraint due to installed dc link converter capacity. Furthermore, if the power sharing algorithm is not dynamically employed, the parallel ac-dc link system will inevitable operate at a sub-optimal efficiency point over its operational lifetime, thus incurring avoidable losses. The impact of Δy on system losses ($\Delta P_{\text{L,sys}}$) is a function of operating conditions as indicated by (12) and (13), where in a higher slope implies a greater deviation in power losses from its minimum. The inferences

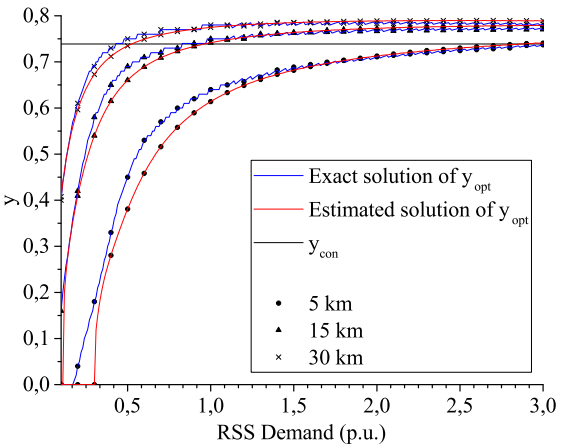

Fig. 6: Analytically estimated y_{opt} as compared to its exact solution with varying S_{RSS} at pf=0.9 for different link lengths.

TABLE I: Tendencies in y_{opt} and $\Delta P_{\text{L,sys}}$ with varying system conditions (↑ indicates increase and ↓ a decrease as the associated parameter increases).

	S_{RSS}	$V_{\text{LL,rms}}$	k_{e}	η	l	A_{con}
y_{opt}	↑	↓	↑	↑	↑	↓
$\Delta P_{\text{L,sys}}$	↑	↓	↓	↓	↑	↓

associated with the tendencies of y_{opt} (from (17)) and $\Delta P_{\text{L,sys}}$ (from (12),(13)) are summarized in Table I.

The inference supports the intuitive understanding that considering all other factors constant, if increase in a specified parameter implies a more efficient dc operation relative to the ac link, y_{opt} increases. Further, if this improves the efficiency of the overall system, $\Delta P_{\text{L,sys}}$ decreases. For example, an increase in η makes the dc link more efficient relative to the ac link if all other factors are assumed constant. Therefore, y_{opt} increases but $\Delta P_{\text{L,sys}}$ decreases. Considering that an increase in link length l results in a greater increase in ac link losses as compared to the dc link, y_{opt} increases. However, since the overall system losses increase, $\Delta P_{\text{L,sys}}$ increases in this case. An accurate knowledge of y_{opt} is important from power steering control point of view, as shall be explored in Section IV.

IV. Developed Algorithm and Simulated Dynamic Performance

The flow diagram showing the developed algorithm for estimation of y_{opt} is shown in Fig. 7. The method is based on the analytic equations derived in Section II and III.

A. Deployment of the Algorithm

The measured values of RSS line voltage ($v_{\text{ll,RSS}}$) and current ($i_{\text{ll,RSS}}$) are used to determine the total RSS power demand (P_{RSS}, Q_{RSS}) in Step 0. In Step 1, the initial estimate ($y(0)$) at iteration i=0 is determined from (7). In step 2 and 3, all the indicated intermediate variables are estimated using the equations highlighted in Fig. 7. The value of y_{opt} at i$^{\text{th}}$ iteration is calculated in step 4 and the process is repeated until

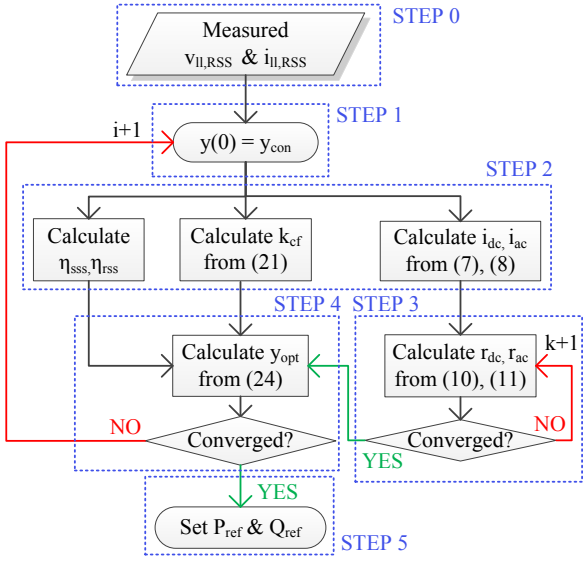

Fig. 7: Algorithm for the estimation of y_{opt} during dynamic system operation of parallel ac-dc distribution links.

the solution converges. The convergence criterion of 1e-6 is used. In the considered scenarios, the estimated y_{opt} converges within the maximum allowed iterations of 5.

Optionally, if the range of operating power demand at RSS is known, Step 1 to 4 can be used to predefine a lookup table for the possible y_{opt}. Finally, the active and reactive power set points (P_{ref},Q_{ref}) for the output current controller of the RSS side converters is determined. The system shown in Fig. 2 is simulated to verify the dynamic working of the developed algorithm. The specific parameters used for the depicted results are listed in Table III.

All ac and dc link conductors are modelled as a resistance in series with a inductance. Substations at each side of the link system has three MMCs of 10 MVA capacity each, corresponding to $k_{cr} = 1$. Each SSS side MMC is responsible for the voltage control of an individual dc link, giving three dc links with dedicated back to back converters in parallel with a single three-phase ac link. The dc link voltage corresponds to a 10 kV ac grid with $k_e = 1.05 * \sqrt{2}$ to comply with the operating limits imposed by the considered arm inductance.

The developed optimal power sharing algorithm is only required at the RSS side MMCs, each of which share one-third of the active and reactive power demand on the dc link system. All the simulated MMCs consist of a PLL, output current controller, circulating current controller and arm energy controllers as described in [25]. The insertion indices of the MMCs are computed using direct voltage control. Specific to parallel ac-dc links simulated in this paper zero sequence currents (ZSC) can externally circulate via the ac and dc links between the B2B-VSC if isolating transformer is not present [26]. The existence and mitigation of such ZSC is explored for parallel operating converters with shared ac and dc buses in [27], [28] . These concepts are applied to develop the ZSC controller for the parallel ac-dc system, as described in [26] and is not the focus of the current paper. A detailed information on this topic can be found in [29]–[34].

The two suggested deployment methods (i) iterative estimation (ii) pre-defined lookup table where converter controllers rely on the locally measured three-phase voltages and current load at RSS for optimally steering the active power while supporting the full reactive power demand. If the parallel ac-dc link architecture is reconfigurable, as suggested in [6], the information on the operating configuration must be available with the RSS-side controller to correctly employ (17). With communication between SSS and RSS, the accuracy of the suggested method can be improved. The potential of improved accuracy should be weighed in consideration to the amount and resolution of available information. This aspect is beyond the scope of this research. Further, alternate methods such as perturb and observe can be used to find optimal operating efficiency.

B. Simulation Results

The simulation results for optimal power flow control are shown in Fig. 8.

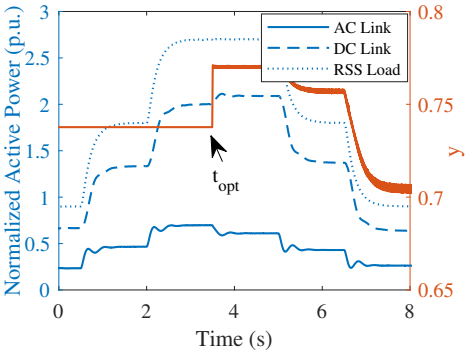

(a)

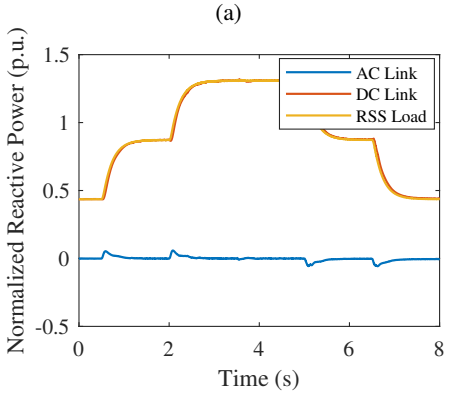

(b)

Fig. 8: Simulation results (a) Active power and y (optimal power sharing algorithm is triggered at time $t = t_{opt}$) (b) Reactive power fully met by the RSS converters.

For time t< t_{opt}, as the RSS load varies from 1 p.u. to 3 p.u. at pf=0.9 corresponding to the base power in Table II, the total active power share of the three dc links corresponds to $y = y_{con}$. For time t> t_{opt}, the output of the y_{opt} algorithm described in Fig. 7 is used to generate the reference powers for the current controllers of the RSS MMCs. It can be observed in Fig. 8a that y decreases with decreasing RSS load, consistent

with the prediction in Fig. 6. The active powers of the ac and dc links correspondingly vary. For the entire period of simulation, the total reactive power demand of the RSS is supported by the three MMCs at the RSS side of the dc link.

V. Case-study for Energy Saving Potential

A. Adapted load profile data

As highlighted previously, the system presented in Fig. 2 is based on the proposed dc refurbishment strategy of an existing 10 kV ac distribution link with physical parameters listed in Table II, as described in [19]. The annual data for the hourly average apparent power demand profile at the RSS of this system is shown in Fig. 9a. The values are shown in p.u. and the profile is adapted such that the peak demand (at 3 p.u.) corresponds to the maximum system capacity during (n-1) contingency. The corresponding exact solution of y_{opt} for a link length of 5 km is shown in Fig. 9b.

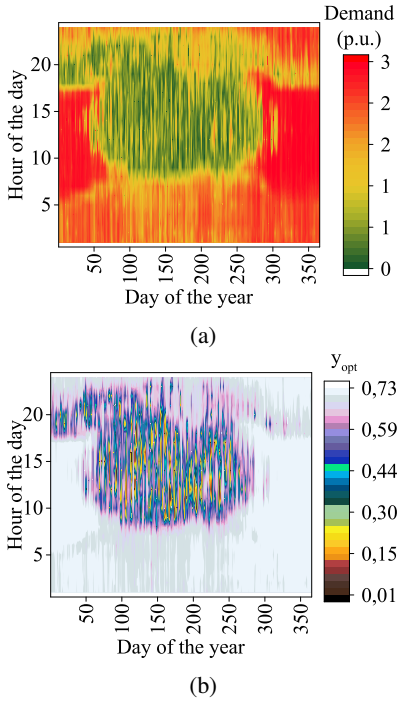

Fig. 9: Case-study (a) Annual hourly average apparent power demand (b) Corresponding y_{opt} for a 10 kV grid voltage with link length and conductor area of 5 km and 630 mm^2 respectively.

It can be observed that the tendency of y_{opt} to increase with demand is consistent with the theory presented in preceding sections. The total system energy loss over one year computed for constant power sharing ratio of y_{con} and optimal ratio y_{opt} is given by $E_{loss,}(y_{con})$ and $E_{loss,}(y_{opt})$, respectively. The annual energy saving potential (ΔE_{loss}) of implementing the optimal efficiency power sharing is thus given by (18).

$$\Delta E_{loss} = E_{loss,}(y_{con}) - E_{loss,}(y_{opt}) \tag{18}$$

B. Dependence of Grid Voltage

ΔE_{loss} as a function of link length for different grid voltages (5 kV, 10 kV, 15 kV and 20 kV) is given in Fig. 10. Note that the demand profile is the same as Fig. 9a in p.u. for all cases. For a given grid voltage, the base power is described by $S_{base} = \sqrt{3} V_{LL,rms} I_{cond,rated}$. While the cross-sectional area dependent rated link conductor current is kept constant at 590 A, S_{base} and therefore, the S_{RSS} in MVA varies as a function of grid voltage. Considering that y_{opt} varies as a function of $V_{LL,rms}$, l and S_{RSS}, the observed tendencies in ΔE_{loss} are correspondingly related to the simultaneous impact of these parameters.

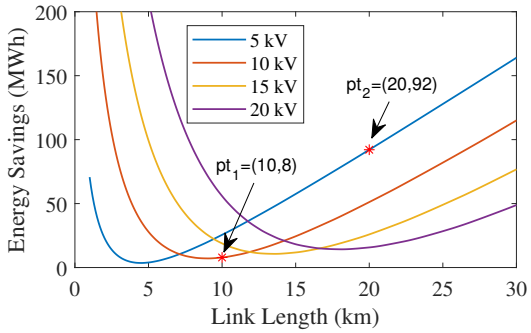

Fig. 10: Energy Saving potential as a function of link length for different ac grid voltages.

It can be observed that for a given $V_{LL,rms}$ (and thus fixed S_{RSS} MVA demand profile), ΔE_{loss} saving potential has a minimum at a certain link length ($l_{\Delta Eloss,min}$). This tendency is an effect of variation in y_{opt} and the cumulative impact of $\Delta P_{L,sys}$ at various operating points over the year in accordance with Table I. In the range $l < l_{\Delta Eloss,min}$, y_{opt} increases with link length from a magnitude relatively lower than y_{con}. This results in a net reduction in ΔE_{loss} with increasing l, even though $\Delta P_{L,sys}$ has an increasing tendency. In the range $l > l_{\Delta Eloss,min}$, y_{opt} is greater than y_{con} for relatively high RSS power demand and the slope of its variation reduces with l (refer Fig. 6). Therefore, ΔE_{loss} increase due to the cumulative impact of the variation in y_{opt} relative to y_{con} and the increase in $\Delta P_{L,sys}$ due to increase in l. Finally, the energy savings increase with grid voltage for short link lengths, while decrease with increasing grid voltage for relatively longer link lengths. Furthermore, the $l_{\Delta Eloss,min}$ increases with increasing grid voltage.

C. Dependence of Conductor Area

ΔE_{loss} as a function of link length for different link conductor area (630 mm^2, 400 mm^2, 240 mm^2 and 185 mm^2) is given in Fig. 11. The grid voltage is taken constant at 10 kV and therefore, S_{base} varies as a function of $I_{cond,rated}$. It can be observed that the variation of ΔE_{loss} as a function of link conductor area is relatively less significant as compared to l and $V_{LL,rms}$.

In Fig. 10 and Fig. 11, the depicted points pt_1, pt_2 and pt_3 show that energy saving potential of 8-92 MW exists for range of link length between 10-20 km, grid voltage 5-20 kV and conductor cross-sectional area of 185-630 mm^2. The expected savings can be extrapolated based on the tendencies highlighted in the preceding discussion.

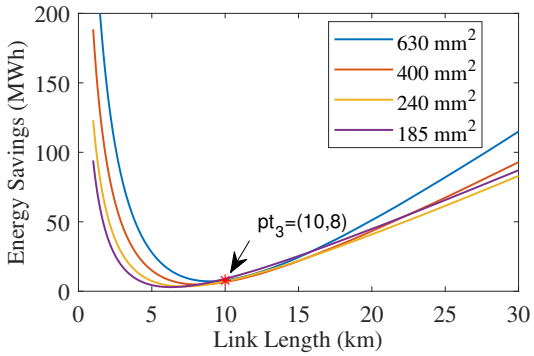

Fig. 11: Energy Saving potential as a function of link length for different link conductor area.

D. Error Analysis

The practical parameters are different than the theoretically estimated values, leading to deviation Δy from the actual y_{opt}.The source of this error is a cumulative impact of the estimation error for the parameters in (17). Fig. 12 and Fig. 13 show the additional losses incurred annually by a deviation of Δy=5 % and Δy=3 % for different link lengths, grid voltage and conductor cross-sectional area respectively.

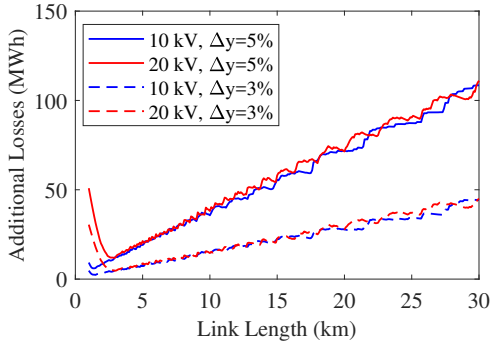

Fig. 12: Additional losses due to sub-optimal y as a function of link length for different ac grid voltages.

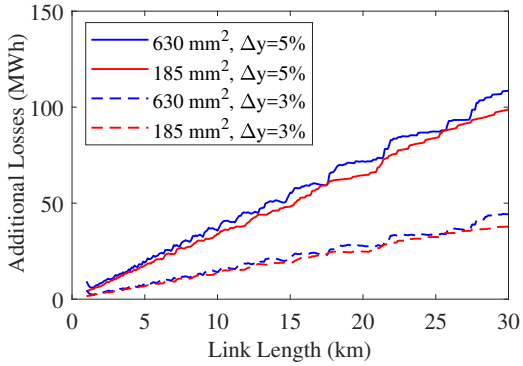

Fig. 13: Additional losses due to sub-optimal y as a function of link length for different cross-sectional area.

It can be observed that the incurred losses increase with link length but are less sensitive to variation in grid voltage and cross-sectional area. These tendencies of the estimation error in y_{opt} and its corresponding impact on actual system losses should be compared with the potential energy savings for the given operational conditions as highlighted in the preceding sections. If marginally positive or negative change in system efficiency is expected, the option of operating the system at y_{con} may be considered.

VI. Experimental Results

A. Test Setup

Fig. 14 shows the parallel ac-dc link set-up used to emulate the equivalent circuit shown in Fig. 2.

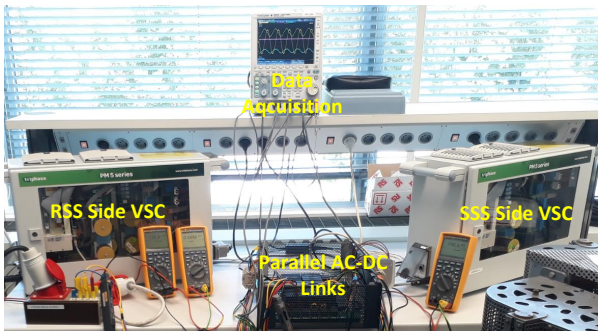

Fig. 14: Test Setup used to validate key control concepts.

2-level voltage sourced converters consisting of three half bridge IGBTs with ac side LCL filter are used in a back-to-back dc link system connected in parallel with the ac link to steer active power from the 3-phase ac source at SSS side to a constant power load (CPL) at RSS side. The parameters of the test converter used in the experimental set-up are given in Table IV.

The conductors of parallel ac and dc links are represented by six resistances R_1-R_6. The switches are connected such that resistances R_1, R_2 and R_3 operate as three phase ac link while resistances R_5 and R_6 operate as positive and negative pole conductors of the dc link respectively. Each ac link conductor resistance is 6 Ω while dc link resistance is 2 Ω such that the operating condition with 3x ac conductors and 6x dc link conductors is emulated in the experiments. An oscilloscope is used to measure the ac link current (i_{ac}), dc link current (i_{dc}) and the output ac current of the VSC at the RSS side of the dc link ($i_{\text{vsc,rss}}$). Further, the line to line voltages of the RSS bus is also measured.

B. Measured waveforms and optimal efficiency

Fig. 15 shows typical waveforms of current and voltages with varying y. The oscilloscope settings are shared in the 'Instrumentation' section in the Appendix. From the waveforms, the actual active power share ratio y can be determined.

It can be observed that the dc link can steer the active power in parallel ac-dc link system for a given load. The measured current waveforms show that the ZSC controller is successfully mitigating the common mode currents even though isolating

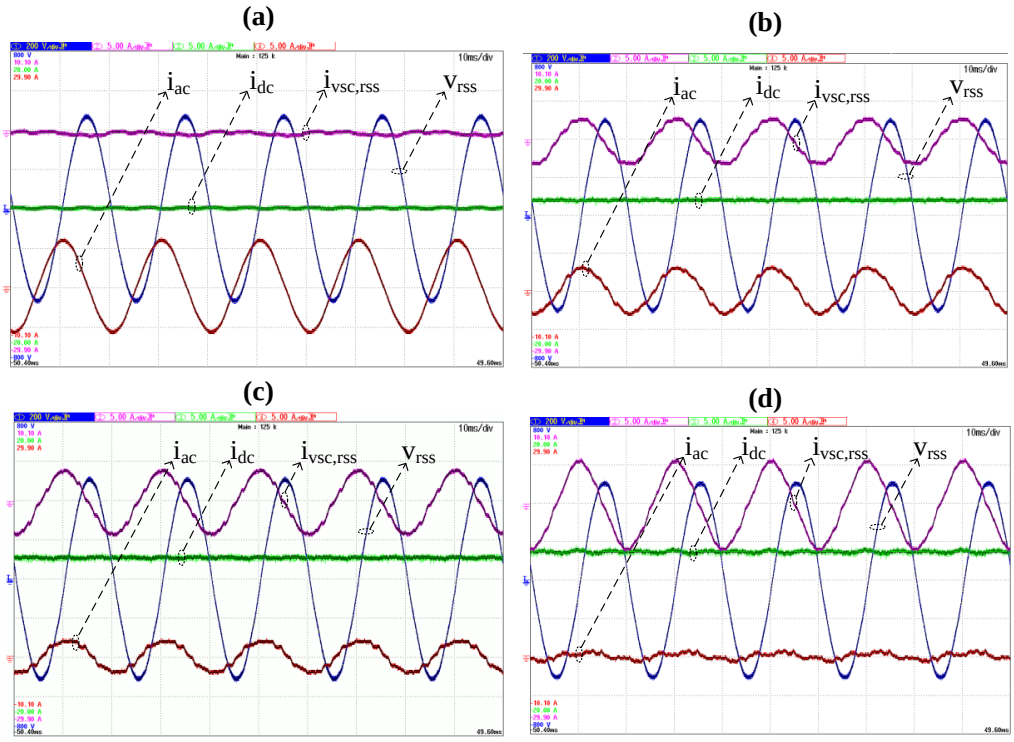

Fig. 15: Measured waveforms of parallel ac-dc link set-up with (a) $y = 0$ (b) $y = 0.52$ (c) $y = 0.68$ (d) $y = 1$.

transformer is not employed between the parallel ac-dc links at RSS. Furthermore, Fig. 15(d) demonstrates the ability of the dc link to reduce the ac link current to near zero. This ability can be utilized for substation bus transfer and online reconfiguration applications in future.

A three-phase power analyzer was installed to measure the power outflow from SSS and RSS node so that operating system efficiency could be determined. Fig. 16 shows the measured system efficiency as a function of y for a RSS load of 3.5 kW (blue) and 4 kW (red).

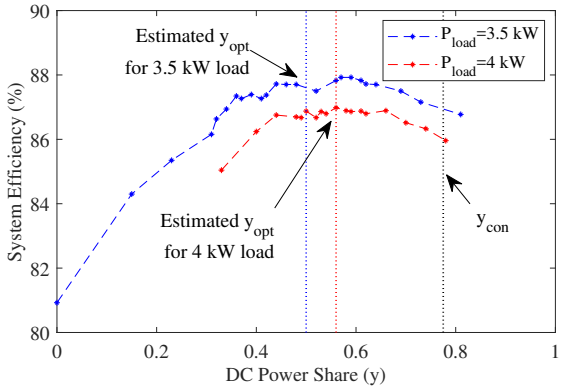

Fig. 16: Measured system efficiency as a function of y.

Note that as the share of dc link power increases for a given load power, the RSS side voltage increase due to lower voltage drop in the ac link resistances. To keep the power drawn constant, the CPL was used to correct for this effect with varying y. It can be seen that system efficiency reduces both for relatively high and low values of y, giving an optimal sharing point as discussed in Section III. The theoretical estimate of y_{opt} and y_{con} considering converter efficiency at 94 % is highlighted. It can be observed that the system efficiency is lower if the power sharing is decided based on the thermal capacity of the ac and dc link conductors.

This optimal point shifts with operational conditions. For example, it can be observed from Fig. 16 that when load power increases from 3.5 kW to 4 kW, the measured optimal efficiency power sharing ratio increases, consistent with the theory presented in Section III.

C. Critical Comparison

It can be observed in Figure 16 that at 4 kW, the maximum system efficiency of 86.68 % is measured at $y = 0.56$ and corresponds with the theoretically estimated value. However, at lower power of 3.5 kW, the maximum efficiency is at a slightly higher y as compared to the theoretical value. This deviation can be attributed to individual power-efficiency curves of the SSS and RSS VSCs. While measured converter efficiency curves can improve estimation accuracy at lower operating powers, this can increase the computational complexity and/or communication requirements. It is necessary to weigh this operational trade-off against the achieved benefit, for example an improvement of system efficiency by 0.3 % in this test result.

VII. Conclusion and Future Work

This paper proves that a back to back dc link can be operated in parallel with an ac distribution link to optimally

steer the active power while supporting the full reactive power at receiving end. The specific conclusions are as follows:

- The derived analytical expression suggests that the optimal dc to ac link active power sharing ratio y_{opt} increases with increase in total power demand, link length, converter efficiency and dc to ac voltage enhancement ratio, while decreases with conductor area and ac grid voltage. With deviation in system operating point from this optimal ratio, the additional system losses tend to decrease with increase in ac grid voltage, dc to ac voltage enhancement ratio, converter efficiency and conductor area, while increase with power demand and link length.
- Sensitivity analysis on the above mentioned operating parameters with adapted data from a practical grid case-study indicates the trends in the competing influence of these variations on y_{opt} and $\Delta P_{\text{L,sys}}$ as compared to benchmark y_{con}. It is shown that annual energy saving potential in the range of 8-92 MWh can be achieved with varying link length between 10-20 km for grid voltages of 5-20 kV and conductor area of 185-630 mm^2. A quantified discussion on the additional incurred losses due to estimation error in y_{opt} is offered.
- The described deployment of the power flow algorithm is simulated to show that the dc link converter can steer the active power in the point to point parallel ac-dc link at optimal efficiency while supporting the full reactive power using local measurements of voltage and current at receiving end.
- Experimental results indicate that the converters can steer the active powers in the system without generating common mode currents in the absence of isolating transformer. The efficiency measurements support the theoretically inferred tendencies in y. It was observed that estimation error tends to increase as compared to the actual measured optimal at lower operating powers, consistent with the theoretical expectations.

As part of future work, reconfigurability between the ac and dc link conductors can be explored to demonstrate the proper working of the algorithm under such operation. The experimentally demonstrated power steering capability can be utilized to realize near-zero current online reconfigurations to optimize power flows in the system.

APPENDIX

A. System Paramters

Table II lists the test parameters used for the presented results, unless specified otherwise.

TABLE II: Test Network Parameters

$V_{\text{LL,rms}}$	10 kV
Type of conductor	Aluminum
A_{con}	630 mm^2
Rated conductor current	590 A
N_{ac}, N_{dc}	3, 6
Capacity during (n-1) contingencies	3 p.u. at pf=0.9
Base Power	10.2 MVA

B. Parameters for Simulation Results

The parameters used for simulation results in Section IV are shown in Table III.

TABLE III: Specific converter and system parameters for the depicted simulation results(based on [21], [23]).

Converters per substation	3
Per Converter Capacity	10 MVA
Submodule capacitance	3.3 mF
Arm inductance	3 mH
Arm Resistance	0.1 Ω
DC Link Capacitance	100 μF
DC link voltage	17.14 kV
Conductor Resistance	65 $m\Omega$/km
Conductor Inductance	0.55 mH/km
Link length	10 km

C. Parameters for Experimental Set-up

The converter parameters used in the experimental set-up are shown in Table IV.

TABLE IV: Parameters of the VSC used in the experimental set-up.

Parameter	**Value**
Rated Power	5 kVA
AC Grid Voltage	400 V (r.m.s)
Grid Side Inductance	1.5 mH
Grid Side Resistance	0.2 Ω
Filter Capacitance	20 μF
Converter Side Inductance	1.5 mH
Converter Side Resistance	0.2 Ω
DC-Side Voltage	750 V
DC Pole-to-Pole Capacitance	500 μF

D. Instrumentation

There are 8 sensors are provided per converter as discussed in [35]. These include 3 current sensors at the ac grid side, 2 differential voltage sensors at the ac grid providing phase to phase voltages, 2 current sensors at the inverter end and 1 differential direct voltage sensor.

A DLM2000 oscilloscope with sample rate of 1250000 s^{-1} is used to measure the RSS voltage (Ch1, blue, 200 V/div), output ac current of RSS VSC (CH2, pink, 5 A/div), dc link current (CH3, green, 5 A/div) and ac link current (CH4, red, 5 A/div). Time resolution of 10 ms/div is used.

The system efficiency is measured using two 3-phase NANOVIP PLUS power analyzers, one to measure the input power and the other to measure the output load power. The input channels include two voltage probes with a maximum of 600 V ac (20 Hz -600 Hz) and a current measurement. Fixed sampling is used at a frequency of 1.25 kHz and the measurement rate is 1 s in normal operation. The minimum measurable signal is 1 V with a resolution of 480 mV for a 750 V$_{\text{rms}}$ range. A full discussion on the characteristics of the device is offered in [36].

REFERENCES

[1] "MVDC plus medium voltage direct current - managing the future grid," *Siemens AG*, 2017.

[2] M. Liserre, G. Buticchi, M. Andresen, G. De Carne, L. F. Costa, and Z. Zou, "The smart transformer: Impact on the electric grid and technology challenges," *IEEE Industrial Electronics Magazine*, vol. 10, DOI 10.1109/MIE.2016.2551418, no. 2, pp. 46–58, Jun. 2016.

[3] S. K. Chaudhary, J. M. Guerrero, and R. Teodorescu, "Enhancing the capacity of the ac distribution system using dc interlinks: A step toward future dc grid," *IEEE Transactions on Smart Grid*, vol. 6, DOI 10.1109/TSG.2015.2404313, no. 4, pp. 1722–1729, Jul. 2015.

[4] R. T. Pinto, M. Aragues-Penalba, O. Gomis-Bellmunt, and A. Sumper, "Optimal operation of dc networks to support power system outage management," *IEEE Transactions on Smart Grid*, vol. 7, DOI 10.1109/TSG.2016.2586024, no. 6, pp. 2953–2961, Nov. 2016.

[5] S. I. Nanou and S. A. Papathanassiou, "Frequency control of island vsc-hvdc links operating in parallel with ac interconnectors and on-site generation," *IEEE Transactions on Power Delivery*, vol. 33, DOI 10.1109/TPWRD.2017.2722498, no. 1, pp. 447–454, Feb. 2018.

[6] A. Shekhar, L. M. Ramirez-Elizondo, T. B. Soeiro, and P. Bauer, "Boundaries of operation for refurbished parallel ac-dc reconfigurable links in distribution grids," *IEEE Transactions on Power Delivery*, DOI 10.1109/TPWRD.2019.2915198, pp. 1–1, 2019.

[7] L. Zhang, J. Liang, W. Tang, G. Li, Y. Cai, and W. Sheng, "Converting ac converting ac distribution lines to dc to increase transfer capacities and dg penetration," *IEEE Transactions on Smart Grid*, DOI 10.1109/TSG.2017.2768392, pp. 1–1, 2018.

[8] A. Shekhar, E. Kontos, L. Ramírez-Elizondo, A. Rodrigo-Mor, and P. Bauer, "Grid capacity and efficiency enhancement by operating medium voltage ac cables as dc links with modular multilevel converters," *International Journal of Electrical Power Energy Systems*, vol. 93, DOI https://doi.org/10.1016/j.ijepes.2017.06.012, pp. 479 – 493, 2017.

[9] C. Tang, Y. Chen, Y. Chen, and Y. Chang, "Dc-link voltage control strategy for three-phase back-to-back active power conditioners," *IEEE Transactions on Industrial Electronics*, vol. 62, DOI 10.1109/TIE.2015.2420671, no. 10, pp. 6306–6316, Oct. 2015.

[10] L. Zhang, L. Harnefors, and H. Nee, "Interconnection of two very weak ac systems by vsc-hvdc links using power-synchronization control," *IEEE Transactions on Power Systems*, vol. 26, DOI 10.1109/TPWRS.2010.2047875, no. 1, pp. 344–355, Feb. 2011.

[11] P. Khamphakdi, K. Sekiguchi, M. Hagiwara, and H. Akagi, "A transformerless back-to-back (btb) system using modular multilevel cascade converters for power distribution systems," *IEEE Transactions on Power Electronics*, vol. 30, no. 4, pp. 1866–1875, Apr. 2015.

[12] K. Sekiguchi, P. Khamphakdi, M. Hagiwara, and H. Akagi, "A grid-level high-power btb (back-to-back) system using modular multilevel cascade converters withoutcommon dc-link capacitor," *IEEE Transactions on Industry Applications*, vol. 50, DOI 10.1109/TIA.2013.2290867, no. 4, pp. 2648–2659, Jul. 2014.

[13] J. Teng, S. Liao, W. Huang, and C. Chiang, "Smart control strategy for conversion efficiency enhancement of parallel inverters at light loads," *IEEE Transactions on Industrial Electronics*, vol. 63, DOI 10.1109/TIE.2016.2594791, no. 12, pp. 7586–7596, Dec. 2016.

[14] H. Ergun, J. Dave, D. Van Hertem, and F. Geth, "Optimal power flow for acâdc grids: Formulation, convex relaxation, linear approximation, and implementation," *IEEE Transactions on Power Systems*, vol. 34, DOI 10.1109/TPWRS.2019.2897835, no. 4, pp. 2980–2990, Jul. 2019.

[15] L. Zhang, Y. Chen, C. Shen, W. Tang, J. Liang, and B. Xu, "Optimal configuration of hybrid ac/dc urban distribution networks for high penetration renewable energy," *IET Generation, Transmission Distribution*, vol. 12, DOI 10.1049/iet-gtd.2018.5722, no. 20, pp. 4499–4506, 2018.

[16] H. M. A. Ahmed and M. M. A. Salama, "Energy management of acâdc hybrid distribution systems considering network reconfiguration," *IEEE Transactions on Power Systems*, vol. 34, DOI 10.1109/TPWRS.2019.2916227, no. 6, pp. 4583–4594, Nov. 2019.

[17] C. Qi, K. Wang, Y. Fu, G. Li, B. Han, R. Huang, and T. Pu, "A decentralized optimal operation of ac/dc hybrid distribution grids," *IEEE Transactions on Smart Grid*, vol. 9, DOI 10.1109/TSG.2017.2703582, no. 6, pp. 6095–6105, Nov. 2018.

[18] N. Meyer-Huebner, M. Suriyah, and T. Leibfried, "Distributed optimal power flow in hybrid acâdc grids," *IEEE Transactions on Power Systems*,

[19] A. Shekhar, E. Kontos, L. Ramírez-Elizondo, and P. Bauer, "Ac distribution grid reconfiguration using flexible dc link architecture for vol. 34, DOI 10.1109/TPWRS.2019.2892240, no. 4, pp. 2937–2946, Jul. 2019.
increasing power delivery capacity during (n-1) contingency," *IEEE Southern Power Electronics Conference (SPEC)*, 2017.

[20] R. Alvarez, M. Wahle, H. Gambach, and J. Dorn, "Optimum semiconductor voltage level for mmc submodules in hvdc applications," in *2016 18th European Conference on Power Electronics and Applications (EPE'16 ECCE Europe)*, pp. 1–9, Sep. 2016.

[21] J. E. Huber and J. W. Kolar, "Optimum number of cascaded cells for high-power medium-voltage ac-dc converters," *IEEE Journal of Emerging and Selected Topics in Power Electronics*, vol. 5, DOI 10.1109/JESTPE.2016.2605702, no. 1, pp. 213–232, Mar. 2017.

[22] S. Rodrigues, A. Papadopoulos, E. Kontos, T. Todorcevic, and P. Bauer, "Steady-state loss model of half-bridge modular multilevel converters," *IEEE Transactions on Industry Applications*, vol. 52, DOI 10.1109/TIA.2016.2519510, no. 3, pp. 2415–2425, May. 2016.

[23] A. Shekhar, L. B. Larumbe, T. B. Soeiro, Y. Wu, and P. Bauer, "Number of levels, arm inductance and modulation trade-offs for high power medium voltage grid-connected modular multilevel converters," in *2019 10th International Conference on Power Electronics and ECCE Asia (ICPE 2019 - ECCE Asia)*, pp. 1–8, May. 2019.

[24] A. Shekhar, T. B. Soeiro, Z. Qin, L. Ramírez-Elizondo, and P. Bauer, "Suitable submodule switch rating for modular multilevel converter design in medium voltage applications," *IEEE Energy Conversion Congress and Exposition (ECCE)*, 2018.

[25] K. Sharifabadi, L. Harnefors, H.-P. Nee, S. Norrga, and R. Teodorescu, *Dynamics and Control*. IEEE, 2016. [Online]. Available: https://ieeexplore.ieee.org/document/7656771

[26] A. Shekhar, T. B. Soeiro, L. Ramırez-Elizondo, and P. Bauer, "Zero sequence currents externally circulating between the back to back modular multilevel converters in parallel ac-dc distribution links," *IEEE 10th International Conference on Power Electronics-ECCE Asia (ICPE-ECCE Asia)*, May. 2019.

[27] C. Pan and Y. Liao, "Modeling and coordinate control of circulating currents in parallel three-phase boost rectifiers," *IEEE Transactions on Industrial Electronics*, vol. 54, DOI 10.1109/TIE.2007.891776, no. 2, pp. 825–838, Apr. 2007.

[28] F. Gao, D. Niu, H. Tian, C. Jia, N. Li, and Y. Zhao, "Control of parallel-connected modular multilevel converters," *IEEE Transactions on Power Electronics*, vol. 30, DOI 10.1109/TPEL.2014.2313333, no. 1, pp. 372–386, Jan. 2015.

[29] J. S. Siva Prasad and G. Narayanan, "Minimization of grid current distortion in parallel-connected converters through carrier interleaving," *IEEE Transactions on Industrial Electronics*, vol. 61, DOI 10.1109/TIE.2013.2245620, no. 1, pp. 76–91, Jan. 2014.

[30] J. S. S. Prasad, R. Ghosh, and G. Narayanan, "Common-mode injection pwm for parallel converters," *IEEE Transactions on Industrial Electronics*, vol. 62, no. 2, pp. 789–794, Feb. 2015.

[31] B. Wei, J. M. Guerrero, J. C. VÃ¡squez, and X. Guo, "A circulating-current suppression method for parallel-connected voltage-source inverters with common dc and ac buses," *IEEE Transactions on Industry Applications*, vol. 53, DOI 10.1109/TIA.2017.2681620, no. 4, pp. 3758–3769, Jul. 2017.

[32] T. Chen, "Zero-sequence circulating current reduction method for parallel hepwm inverters between ac bus and dc bus," *IEEE Transactions on Industrial Electronics*, vol. 59, DOI 10.1109/TIE.2011.2106102, no. 1, pp. 290–300, Jan. 2012.

[33] J. Wang, F. Hu, W. Jiang, W. Wang, and Y. Gao, "Investigation of zero sequence circulating current suppression for parallel three-phase grid-connected converters without communication," *IEEE Transactions on Industrial Electronics*, vol. 65, DOI 10.1109/TIE.2018.2798613, no. 10, pp. 7620–7629, Oct. 2018.

[34] W. Jiang, W. Ma, J. Wang, W. Wang, X. Zhang, and L. Wang, "Suppression of zero sequence circulating current for parallel three-phase grid-connected converters using hybrid modulation strategy," *IEEE Transactions on Industrial Electronics*, vol. 65, DOI 10.1109/TIE.2017.2750625, no. 4, pp. 3017–3026, Apr. 2018.

[35] R. Teixeira Pinto, "Multi-terminal dc networks System integration, dynamics and control," *Delft University of Technology, Phd Thesis*, 2014.

[36] Datasheet, "Nanovip three-phase analyzer," *https://www.elcomponent.co.uk/wp-content/uploads/2018/05/Nanovip$_N$ano$Plus_U$ser $-$ $Manual.pdf$*.